

Thermodynamics of Three-phase Equilibrium in Lennard-Jones System with a Simplified Equation of State

KATAOKA, Yosuke / 山田, 祐理 / 片岡, 洋右 / YAMADA, Yuri

(出版者 / Publisher)

法政大学情報メディア教育研究センター

(雑誌名 / Journal or Publication Title)

法政大学情報メディア教育研究センター研究報告

(巻 / Volume)

28

(開始ページ / Start Page)

23

(終了ページ / End Page)

37

(発行年 / Year)

2014

(URL)

<https://doi.org/10.15002/00009848>

Thermodynamics of Three-phase Equilibrium in Lennard–Jones System with a Simplified Equation of State

Yosuke Kataoka¹⁾ and Yuri Yamada²⁾

¹⁾ *Department of Chemical Science and Technology, Faculty of Bioscience and Applied Chemistry, Hosei University, 3-7-2 Kajino-cho, Koganei, Tokyo 184-8584, Japan, yosuke.kataoka.7t@stu.hosei.ac.jp*

²⁾ *Department of Chemical Science and Technology, Faculty of Bioscience and Applied Chemistry, Hosei University, 3-7-2 Kajino-cho, Koganei, Tokyo 184-8584, Japan, yuri.yamada.gk@k.hosei.ac.jp*

SUMMARY

Simplified equations of state (EOS) are proposed for Lennard–Jones system. This is a model for argon and consisting of single spherical molecules. Molecular dynamics simulations of this system were performed to investigate the temperature and density dependencies of the internal energy and pressure for the gas, liquid, solid, and supercooled liquid states. The internal energy and pressure displayed a near-linear dependency on temperature at a fixed volume. The temperature-dependent term of the average potential energy was assumed to be a linear function of temperature as in the harmonic oscillator.

KEY WORDS: equation of state, phase diagram, triple point, perfect solid, perfect liquid

1. INTRODUCTION

A three-phase equilibrium can typically be studied by a Lennard–Jones (LJ) system [1], for which a perfect solid in contact with a perfect liquid may serve as an idealized model. Various simplified equations of state (EOS) can be used to calculate the Gibbs energy of phase transitions between the solid, liquid, and gas phases based on such a model [2-8]. A simplified EOS that incorporates the harmonic oscillator concept is introduced in this work.

When using a harmonic oscillator approximation, the internal energy of the solid phase (U) is expressed by Eq. (1):

$$U(V, T) = \frac{3}{2} NkT + U_e(V, 0 \text{ K}) + \frac{3}{2} NkT, \quad (1)$$

where V is the volume of the system, T is the temperature, N is the number of spherical atomic or molecular species, and k is the Boltzmann constant. At low temperatures, the most important term in this equation is the average potential energy (U_e). The first term on the right-hand side in Eq. (1) represents the average kinetic energy while the last term is the average potential energy based on the harmonic oscillator approximation.

When using this approximation, the pressure (p) of a solid may be expressed as the volume derivative of the average potential energy at the low temperature limit, and the temperature effect may be expressed as a linear function of temperature as in Eq. (2):

$$p(V, T) = \frac{NkT}{V} - \left(\frac{\partial U_e(V, 0 \text{ K})}{\partial V} \right)_T + \frac{6NkT}{V}. \quad (2)$$

The numerical coefficient of six in the last term of Eq. (2) results from the FCC structure of solid argon [2]. The temperature-dependent terms in Eq. (2) and in the U_e term are valid only for the case of a harmonic FCC

lattice. These equations may be generalized by applying suitable coefficient functions, $f(V)$ and $g(V)$, which can be obtained by fitting molecular dynamics (MD) [9] results as linear functions of temperature, as seen in Eqs. (3) and (4):

$$U(V, T) = \frac{3}{2} NkT + U_e(V, 0K) + g(V)NkT, \quad (3)$$

$$p = \frac{NkT}{V} - \left(\frac{\partial U_e(V, 0K)}{\partial V} \right)_T + f(V)NkT + \left(\frac{dg(V)}{dV} \right) NkT \ln(kT). \quad (4)$$

Here, $g(V)$ and $f(V)$ are functions of the volume obtained by analysis of MD results, while the last term in Eq. (4) is included to satisfy the thermodynamic equation of state [1]. These functions account for the effects of non-harmonic motion near the most stable portions of the solid structure. Over a wide density range, these functions represent interpolations between the condensed and gas phases and are also expected to serve a similar purpose in the liquid phase.

In this paper, the functions $f(V)$ and $g(V)$ will be very simplified as follows.

$$f(V) = \frac{6}{V} \frac{\sigma^3}{v}, v \equiv \frac{V}{N}, \quad (5)$$

$$g(V) = \frac{3}{2} \frac{\sigma^3}{v}. \quad (6)$$

Here, v is the volume per particle and the σ^3/v factor is the number density, which acts as a weighting function that accounts for dense regions of the argon. This factor also interpolates between the condensed and gas phases where the oscillator behavior vanishes. Eqs. (5) and (6) are adapted because these are the simplest ones. None-linear functions of the number density for the coefficients are used in the previous work [7]. In this work we try to see whether the linear functions are allowed in EOS to show the three-phase equilibrium in LJ system.

Many studies have examined the EOS of Lennard–Jones systems [10–13]. Such studies are typically based on MD and Monte Carlo (MC) simulations of the equilibrium state [9] and the EOS thus obtained are used to investigate the gas–liquid and solid–liquid equilibria. Phase equilibria have been studied using both equilibrium and non-equilibrium molecular simulation techniques [14–20], both of which provide reasonably accurate results. The EOS results obtained in this work are compared with these previous simulation results [14–20].

For a comparison of the present calculations with the experimental results on argon, Lennard–Jones parameters are estimated by the critical temperature and the critical density obtained by molecular dynamics [18] and macroscopic observations [1].

2. ANALYSIS OF MD SIMULATIONS

MD simulations [9] were performed to obtain the temperature and density dependencies of the internal energy and pressure using the Fujitsu SCIGRESS program. In this work, the interactions of the spherical molecules were assumed to obey the Lennard–Jones relationship [1], such that the Lennard–Jones potential ($u(r)$) is a function of the intermolecular distance (r) using the equation:

$$u(r) = 4\epsilon \left[\left(\frac{\sigma}{r} \right)^{12} - \left(\frac{\sigma}{r} \right)^6 \right], \quad (7)$$

where ε is the depth of the potential well and σ is the separation distance r at which $u(\sigma) = 0$. Herein, we take the value of the ε and σ constants as the units of energy and length, respectively.

Simulations were performed under the NTV ensemble [9] at a number of fixed number densities (N/V) using a system with $N = 256$ and a sufficiently long cut-off distance for calculation of potential energy and pressure (10^{-8} m for argon, LJ parameters for argon will be given below). Figure 1 presents examples of the simulation results. The average potential energy (U_e) and pressure (p) of each phase were fitted by linear functions of the temperature (T) to give Eqs. (8) and (9).

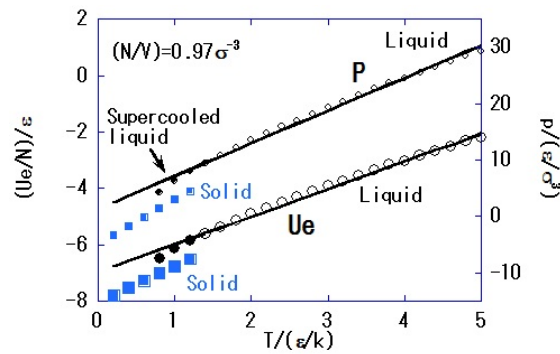


Fig.1 The average potential energy per molecule, U_e/N , and pressure, p , obtained from MD simulations at a number density of $N/V = 0.97 \sigma^{-3}$ as a function of temperature. The solid lines are linear best fits for the liquid phase data.

Although curvature is seen in the liquid data, the linear function of U_e is the most important feature of the harmonic oscillator approximation in this work (Eq.(3)). As the last term in Eq. (4) is understood as a correction term, the pressure is nearly linear as a function temperature in the present approximation.

$$\frac{U_e}{N\varepsilon} = a(U_e) \frac{kT}{\varepsilon} + \frac{U_e(V, 0 \text{ K})}{N\varepsilon}, \quad (8)$$

$$(9)$$

Plots of the variations in the coefficients $a(U_e)$, $a(p)$, and $U_e(V, 0 \text{ K})$ are shown in Figs. 2, 3, and 4. For simplicity, the $a(p)$ and $a(U_e)$ coefficients may also be expressed as functions of $f(v)$ and $g(v)$, as in Eqs. (10) and (11), respectively:

$$a(p, \text{solid}) = 1 + yf(v), \quad a(p, \text{liquid}) = 1 + xf(v), \quad (10)$$

$$a(U_e) = g(v). \quad (11)$$

Here, x and y are adjustable parameters which are determined by setting the critical point and triple point. The constant term $U_e(0 \text{ K})$ in the fitting Eq. (8) has a minimum around a number density of $1 \sigma^{-3}$, as seen in Fig. 4.

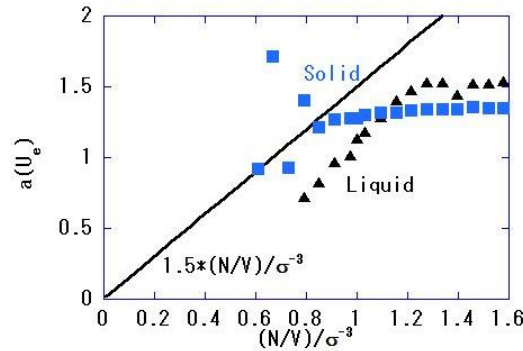


Fig.2 Coefficient $a(U_e)$ as a function of the number density, N/V (see Eq. (8)).

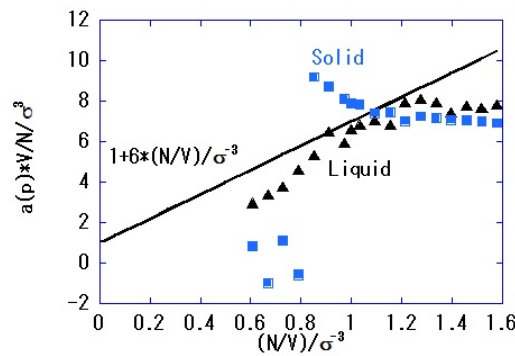


Fig.3 The product of the $a(p)$ coefficient and the volume per molecule, V/N , as a function of the number density, N/V (see Eq. (9)).

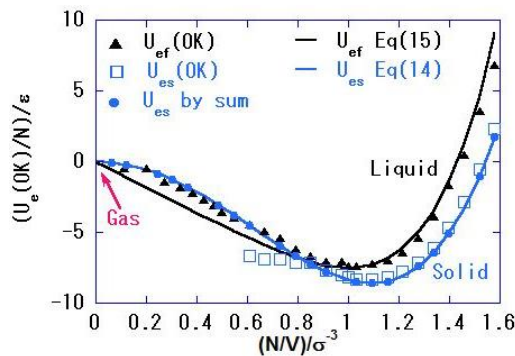


Fig.4 The constant term $U_{es}(0 \text{ K})$ (solid) and $U_{ef}(0 \text{ K})$ (fluid) as a function of the number density, N/V . The sum of the potential energy on the FCC lattice and the functions are also shown (Eqs. (14) and (15)).

3. EQUATIONS OF STATE

The present EOS are as follows [6]:

$$U(V, T) = \frac{3}{2} NkT + U_e(V, 0 \text{ K}) + g(v)NkT \quad (12)$$

$$p(V, T) = \frac{NkT}{V} - \frac{dU_e(V, 0 \text{ K})}{dV} + f(v)NkT + \left(\frac{dg(v)}{dv} \right) NkT \ln(kT), \quad (13)$$

$$\frac{U_{e,s}(V, 0 \text{ K})}{N\epsilon} = 6 \left(1 + \frac{1}{128} \right) \frac{\sigma^{12}}{v^4} - 12 \left(1 + \frac{1}{5} \right) \frac{\sigma^6}{v^2}, \text{ (Solid)} \quad (14)$$

$$\frac{U_{e,f}(V, 0 \text{ K})}{N\epsilon} = \left(1.5 \frac{\sigma^{18}}{v^6} - 9 \frac{\sigma^3}{v} \right), \text{ (Liquid)} \quad (15)$$

$$g_s(v) = g(v), f_s(v) = 1.080032 f(v), \text{ (Solid)} \quad (16)$$

$$g_f(v) = g(v), f_f(v) = 0.9562722 f(v). \text{ (Liquid)} \quad (17)$$

Here, the subscript s indicates the solid state while f refers to the fluid phase. It will be shown that there are both liquid and gas branches in the fluid EOS. In this study, the function $f(v)$ associated with the liquid state includes an adjustable parameter, x , that is chosen, as in Eq. (17), to reproduce the critical point. Another adjustable parameter, y , is chosen to reproduce the triple point, as in Eq. (16). These EOS are considered as the EOS for a perfect solid and liquid. The last term in Eq. (13) is included to ensure that Eq. (12) and Eq. (13) satisfy the thermodynamic EOS [1].

The entropy change was calculated for a reversible isothermal expansion and a heating process at constant volume to the next change of state [1] :

$$(V_i, T_i) \rightarrow (V_f, T_f). \quad (18)$$

This entropy change is expressed as follows:

$$\begin{aligned} \Delta S = & (g(V_f) - g(V_i))Nk + Nk \ln \left(\frac{V_f}{V_i} \right) + (F(V_f) - F(V_i))Nk + (g(V_f) - g(V_i))Nk \ln(kT_i) \\ & + \left(\frac{3}{2}Nk + g(V)Nk \right) \ln \left(\frac{T_f}{T_i} \right) \\ & F(v) = \int f(v)dv \end{aligned} \quad (19)$$

Here, the initial state is shown by Eqs. (20) and (21):

$$T_i = \frac{\epsilon}{k}, \quad V_i = Nv_{\max}, \quad (20)$$

$$S_0 \equiv S_i = g(Nv_{\max})Nk + Nk \ln(Nv_{\max}) + F(Nv_{\max})Nk + \left(\frac{3}{2}Nk + g(Nv_{\max})Nk \right) \ln \left(\frac{\epsilon}{k} \right), \quad (21)$$

where the volume (v_{\max}) is sufficiently large compared with the unit volume σ^3 , and temperature is expressed in units of ϵ/k . The functions $F(V)$ and $g(V)$ are assumed to be zero in the initial state (see Eqs. (16) and (17)) and, as a result, the entropy change has the following form:

$$\begin{aligned} \Delta S(Nv, T) = & \frac{3}{2}Nk \ln \left(\frac{kT}{\epsilon} \right) + Nk \ln \left(\frac{v}{\sigma^3} \right) + F(v)Nk + g(v)Nk \ln \left(\frac{kT}{\epsilon} \right) + g(v)Nk, \\ & F(v) = \int f(v)dv \end{aligned} \quad (22)$$

Hereafter, the entropy change from this S_0 is expressed simply as the entropy (S). We refer henceforth to the present version of the EOS as EOS v7.

4. PHASE EQUILIBRIUM IN T - p SPACE

The LJ parameters in our previous papers are those determined by Cuadros et al [21]. Those parameters shows a little difference in the comparison of the critical temperature T_c and volume V_c , when LJ model is applied to argon. In this work, LJ parameters are chosen to reproduce experimental [1] and MD [18] values of the critical temperature and volume. In the following equations, the macroscopic values for argon appear on the right [1], and the simulation results [18] are given by the middle expressions. The parameters are listed in Table 1.

$$\begin{aligned} T_c &= 1.3207 \varepsilon / k = 150.72 \text{ K} \\ V_c / N &= (1 / 0.316) \sigma^3 = 1.250 \times 10^{-28} \text{ m}^3 \end{aligned} \quad (23)$$

Table 1. Lennard-Jones parameters

$(\varepsilon/k) / \text{K}$	$\varepsilon / 10^{-21} \text{ J}$	$\sigma / 10^{-10} \text{ m}$	$(\varepsilon/\sigma^3) / \text{MPa}$	$(\varepsilon/\sigma^3) / \text{atm}$
114.12	1.5475	3.405	39.9	394

The liquid-gas critical point in EOS v7 was determined by numerical solution of Eq. (24) [1]:

$$\left(\frac{\partial p}{\partial V} \right)_T = \left(\frac{\partial^2 p}{\partial V^2} \right)_T = 0, \quad (24)$$

where an adjustable parameter, x , is chosen, as in Eq. (17), to reproduce the experimental [1] and MD [18] critical temperature.

Table 2 compares the obtained critical points with experimental results [1] and with values determined by molecular simulation methods [10, 11, 18].

Table 2. Comparison of critical constants of argon by EOS [10, 11], experimental [1] and MD [18].

	$T_c/(\varepsilon/k)$	$p_c/(\varepsilon/\sigma^3)$	V_c/σ^3
EOS v5 (Ref. 7)	1.470	0.247	2.53
EOS v7	1.321	0.227	2.49
EOS (Ref. 10)	1.313	0.13	3.22
EOS (Ref. 11)	1.340	0.141	3.22
MD (Ref. 18)	1.321	0.129	3.16
exp (Ref. 1)	1.321	0.122	3.16

The critical temperature is adjusted with the MD results [18] by the adjustable parameter, x . The calculated critical volume by EOS v7 is in fair agreement with the experimental [1] and simulation results [18], while the critical pressure is rather high in comparison to the experimental result [1]. The overall comparison is satisfactory with respect to the critical constants.

The pressure and average potential energy U_c at the temperature $T = \varepsilon/k$ are compared with previously reported EOS determined by molecular simulations [10, 11] in Fig. 5.

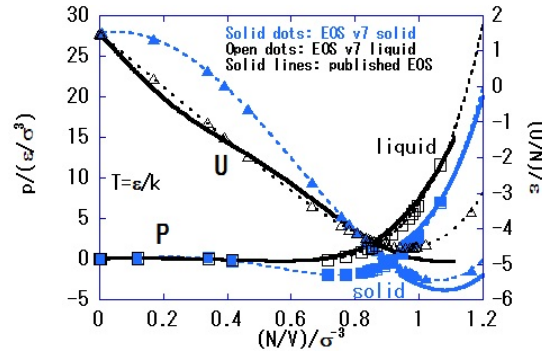


Fig.5 Pressure and internal energy as a function of the number density, plotted for $T = \varepsilon/k$ obtained with EOS v7, in comparison with previously reported EOS [10, 11].

For a given temperature value, T , the phase equilibrium condition between phases 1 and 2 in T - p space may be expressed as:

$$\begin{aligned} p_1(V_1, T) &= p_2(V_2, T), \\ \frac{G_1(V_1, T)}{N_1} &= \frac{G_2(V_2, T)}{N_2}. \end{aligned} \quad (25)$$

Since the EOS are known to be functions of volume and temperature, the above equation can be solved numerically [2, 3], and examples are shown in Figs. 6, 7, and 8 at the triple point.

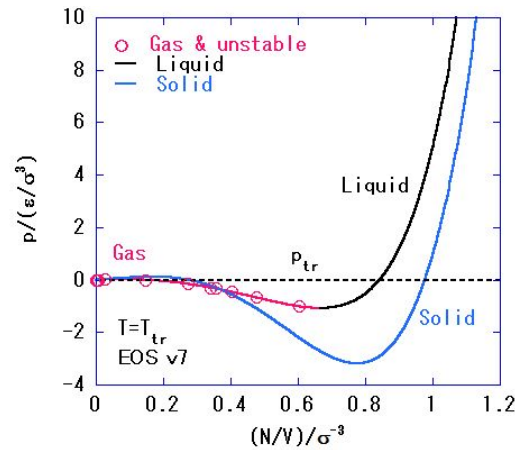


Fig.6 Pressure as a function of the number density, plotted for $T = T_{tr}$. The quantity p_{tr} is the solution of Eq. (25).

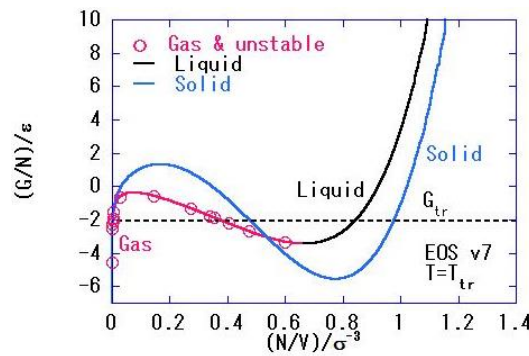


Fig.7 Gibbs energy per molecule, G/N , as a function of the number density, plotted for $T = T_{tr}$. The quantity G_{tr} is the solution of Eq. (25) at this temperature.

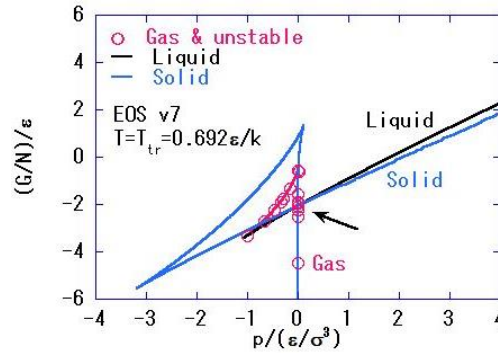


Fig.8 Gibbs energy per molecule, G/N , as a function of pressure at $T_{tr} = 0.692 \epsilon/k$. The arrow indicates the triple point.

Figure 6 demonstrates the density dependence of pressure. The Gibbs energy is plotted as a function of number density (N/V) in Fig. 7. As the pressure decreases, the liquid branch transitions to the gas branch within the van der Waals loop. The solid branch also transitions to the gas branch, and has a slightly higher Gibbs energy than the gas branch originating from the liquid. The adjustable parameter in the function $f_s(v)$ for the solid phase was chosen to reproduce the triple point determined by MC [19]. The calculated thermodynamic properties are summarized and compared with both experimental and simulation results in Table 3, from which it is seen that the calculated properties are a reasonable approximation of the experimental and simulated data.

Table 3. Comparison of triple point with those by EOS v5 [7], MC[15, 18, 19] and experiments[1,22]. The symbol ρ_L and ρ_S stand for the number density of liquid and solid phase.

	$T_{tr}/(\epsilon/k)$	$p_{tr}/(\epsilon/\sigma^3)$	ρ_L/σ^{-3}	ρ_S/σ^{-3}
EOS v5 (Ref. 7)	0.749	2.12E-03	0.845	0.989
EOS v7	0.692	1.66E-03	0.843	0.977
MC (Ref. 15)	0.687	1.10E-02	0.850	0.960
MC (Ref. 18)	0.692	1.21E-03	0.847	0.962
MC (Ref. 19)	0.661	1.80E-03	0.864	0.978
exp (Refs. 1 & 22)	0.734	1.73E-03	0.844	1.01

The calculated transition pressure is plotted as a function of temperature in Fig. 9 and compared with the published EOS [11, 12].

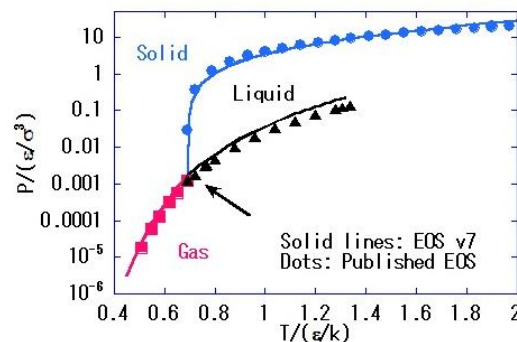


Fig.9 The EOS v7 phase transition pressure as a function of temperature for L-J system compared with the published EOS [11, 12].

The pressure is plotted on a logarithmic scale due to its very wide range. The overall transition pressure for argon is well reproduced as a function of temperature. Figure 10 shows the transition temperature–number density relationship for L-J system and compares the calculated results with the published EOS [11, 12].

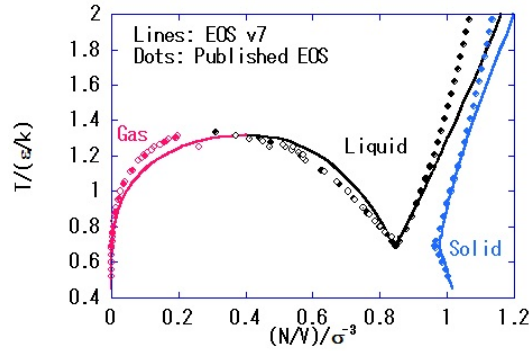


Fig.10 The EOS v7 phase transition temperature as a function of number density, N/V , for L-J system compared with the published EOS [11, 12].

The phase boundaries of the liquid and solid branches obtained from EOS v7 calculations are close to the published results within a temperature range of:

$$0.5 \frac{\varepsilon}{k} \leq T \leq 1.5 \frac{\varepsilon}{k}. \quad (26)$$

The rather large deviations within the high temperature and high-density regions result from the crude approximations in Eqs. (5) and (6). These deviations would not be seen if suitable polynomials were used [7]. Some of the observed differences in the gas–liquid transition are also because of error in the critical volume estimate.

Figure 11 compares the calculated configurational entropy per molecule (S_c/N) with the simulation results [19] in the LJ system.

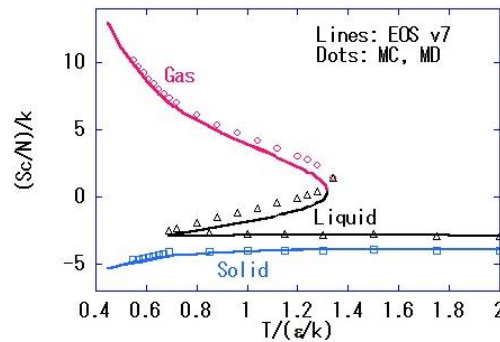


Fig.11 Configurational entropy per molecule, S_c/N , as a function of temperature for the phase equilibrium in LJ system.. Comparison of EOS v7 and simulation results [11,19].

The configurational entropy (S_c) has the following form in the perfect solid and liquid model:

$$S_c(V, T) = Nk \ln \left(\frac{V}{N\sigma^3} \right) + F(v)Nk + g(v)Nk \ln \left(\frac{kT}{\varepsilon} \right) + g(v)Nk + Nk \quad (27)$$

The main feature of the phase equilibrium line in the solid–liquid transition is that the configurational entropies are nearly constant as a function of temperature. This feature is reasonably well reproduced in our plot and therefore the overall features of the configurational entropy plot obtained using EOS v7 are in agreement with the simulation results [19].

Figure 12 presents the average potential energy per molecule (U_c/N) at the phase boundaries, as described by Eq. (28).

$$\begin{aligned}
U_{e,s}(V,T) &= U_{e,s}(V, 0 \text{ K}) + g_s(v)NkT, \text{ (solid)} \\
U_{e,f}(V,T) &= U_{e,f}(V, 0 \text{ K}) + g_f(v)NkT. \text{ (liquid)}
\end{aligned} \tag{28}$$

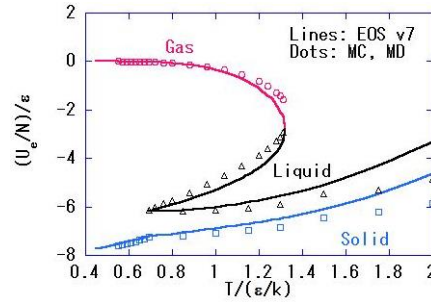


Fig.12 Average potential energy per molecule, U_e/N , as a function of temperature for the phase equilibrium in LJ system. Comparison of EOS v7 and simulation results [11, 19].

These results are also compared with the simulation results [11, 19]. The average potential energies of the solid, liquid and gas generally correspond well with the simulation results within the moderate temperature range defined by Eq. (26). The reason that the average potential energies at liquid–solid equilibrium differ from the observed results for $T > 1.5 \text{ } \epsilon/k$ is seen by the deviation of the MD results from the straight line of $1.5 \text{ } \sigma^3/v$ in the high-density region of Fig. 2.

Figure 13 shows the configurational Helmholtz energy (A_c) as a function of the temperature along the solid–liquid phase boundaries. The calculated A_c value corresponds well with the MC simulation results [19] at low and intermediate temperatures.

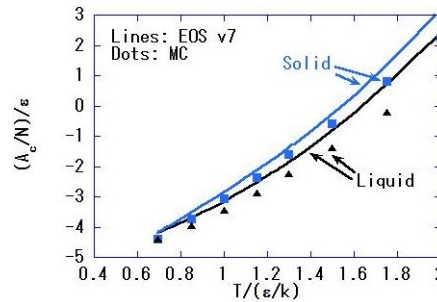


Fig.13 Configurational Helmholtz energy per molecule, A_c/N , as a function of temperature for the solid–liquid equilibrium of LJ system. Comparison of EOS v7 and simulation results [19]

Finally, Fig. 14 compares A_c values at the solid–gas phase boundary with values obtained from MC simulations [19]. EOS v7 gives A_c values on the solid–gas phase boundary that are comparable to those of the MC simulation [19].

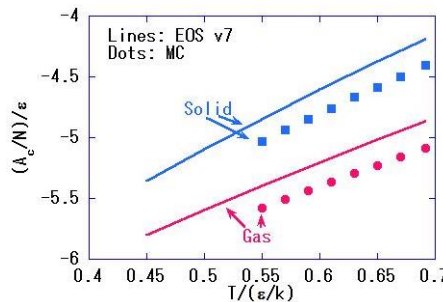


Fig.14 Configurational Helmholtz energy per molecule, A_c/N , as a function of temperature for the solid–gas equilibrium in LJ system. Comparison of EOS v7 and simulation results [19].

5. THERMODYNAMIC PROPERTIES AT A CONSTANT PRESSURE

This section considers thermodynamic quantities at low pressures by comparing the EOS v7 and simulation results. In Fig. 15, the calculated Gibbs energy values are plotted as a function of temperature at $p = 1 \text{ atm} = 3.13 \times 10^{-3} \varepsilon / \sigma^3$.

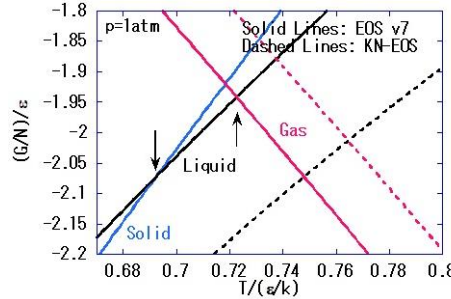


Fig.15 Gibbs energy per molecule, G/N , as a function of temperature at $p = 1 \text{ atm}$. Comparison of EOS v7 and simulation results [10]. The melting point is $0.692 \varepsilon/k$ and the boiling point is $0.723 \varepsilon/k$.

These are compared with the Kolafa–Nezbeda (KN)-EOS data determined from many simulation results for the Lennard–Jones system [11]. The pressure in the MD simulation is 1.2 atm . The MD results are consistent with previous work, [7] while the value of pressure in units of atm is slightly different from the previous work because of the present LJ parameters. When Fig. 15 is considered in detail near the transition points, the comparison is generally satisfactory. The negative liquid and solid entropies result from the present choice of the entropy origin, and, consequently, the Gibbs energy plot differs from its usual form [1]. The melting point (T_m) and the boiling point (T_b) are fixed in Fig. 15 as in Eq. (29).

$$\begin{aligned} T_m &= 79.0 \text{ K} = 0.692 \frac{\varepsilon}{k}, \\ T_b &= 82.5 \text{ K} = 0.723 \frac{\varepsilon}{k}, \\ p &= 1 \text{ atm} = 0.254 \times 10^{-3} \varepsilon / \sigma^3. \end{aligned} \quad (29)$$

These temperatures are close to the macroscopic experimental results [1].

Figure 16 shows the volume per molecule as a function of temperature at $p = 1 \text{ atm}$, compared with the present MD results and the KN-EOS results [11]. The MD simulation was performed on an 864-particle system using a standard NTP ensemble [9]. This comparison demonstrates that the present simple EOS v7 is appropriate.

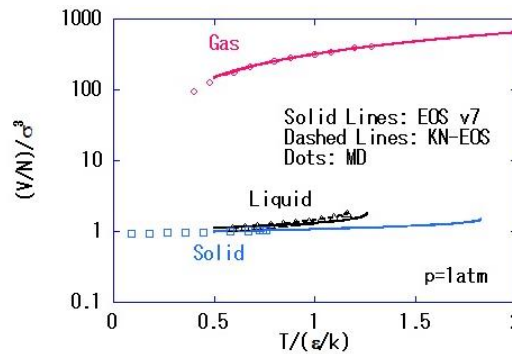


Fig.16 Volume per molecule, V/N , as a function of temperature at $p = 1 \text{ atm}$. EOS v7 results are compared with previous simulation results [11] and the present MD simulations at $p = 1.2 \text{ atm}$.

The internal energy is plotted as a function of temperature at $p = 1 \text{ atm}$ in Fig. 17, where the metastable state

is also included. The stable liquid phase does appear in the region

$$T_m \leq T \leq T_b \quad (30)$$

For this reason, the comparison of the internal energy is satisfactory, as is also the case for the volume data.

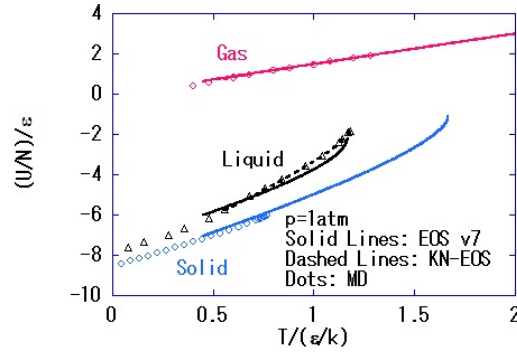


Fig.17 Internal energy per molecule, U/N , as a function of temperature at $p = 1$ atm. EOS v7 results are compared with previous simulation results [11] and the present MD simulations at $p = 1.2$ atm.

Figure 18 depicts the enthalpy per molecule as a function of temperature at $p = 1$ atm. The calculated enthalpy is in agreement with the simulation results for the Lennard–Jones system, while the KN-EOS results are better than EOS v7 in the liquid phase [11].

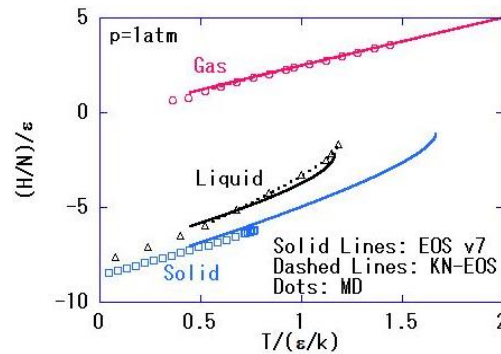


Fig.18 Enthalpy per molecule, H/N , as a function of temperature at $p = 1$ atm. EOS v7 results are compared with previous simulation results [11] and the present MD simulations at $p = 1.2$ atm.

The Helmholtz energy per molecule is shown in Fig. 19 and the entropy per molecule is depicted in Fig. 20.

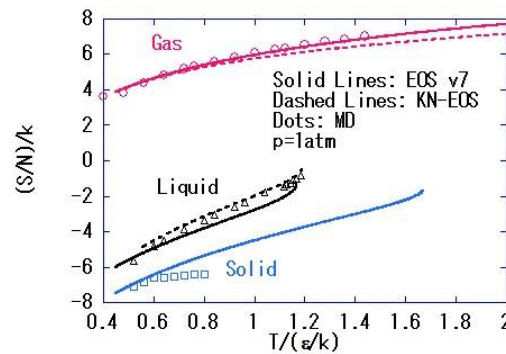


Fig.19 Helmholtz energy per molecule, A/N , as a function of temperature at $p = 1$ atm. Comparison of EOS v7 and simulation results [11].

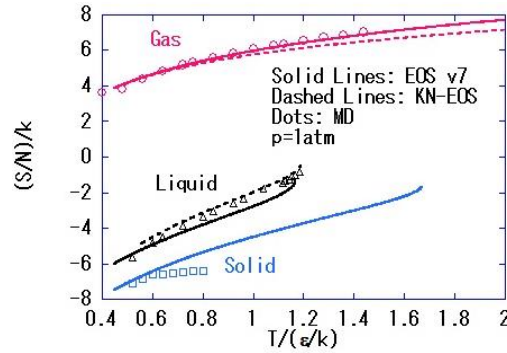


Fig.20 Entropy per molecule, S/N , as a function of temperature at $p = 1$ atm. EOS v7 results are compared with previous simulation results [11] and the present MD simulations at $p = 1.2$ atm. Entropy of the present MD result is calculated by numerical integration of C_p/T and is adjusted with the EOS value at $T = 0.5 \epsilon/k$ at each phase.

The overall features of the Helmholtz energy are satisfactory in comparison with the KN-EOS [11], while the entropy values for the liquid obtained by EOS v7 are close to those obtained from the simulations [11]. The entropies of the liquid and solid are negative based on the present choice of the entropy origin.

Figure 21 compares the expansion coefficient (α) calculated using the EOS with that obtained by MD simulations at $p = 1.2$ atm. Although the EOS v7 α values for the liquid and solid differ slightly from those obtained by the simulations, the overall plots show reasonable similarity. The KN-EOS [11] gives a better expansion coefficient in the liquid phase than the present EOS v7.

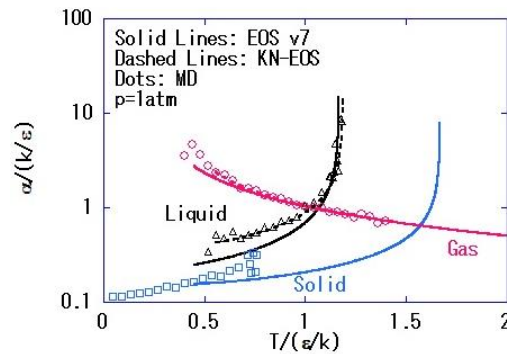


Fig.21 Thermal expansion coefficient, α , as a function of temperature at $p = 1$ atm. EOS v7 results are compared with previous simulation results [11] and the present MD simulations at $p = 1.2$ atm.

The isothermal compressibility (κ_T) at $p = 1$ atm obtained by EOS v7 is plotted in Fig. 22. Comparison of κ_T calculated by the EOS with the MD simulation results indicates that the present EOS satisfactorily explains the order-of-magnitude differences in this term for each of the three phases.

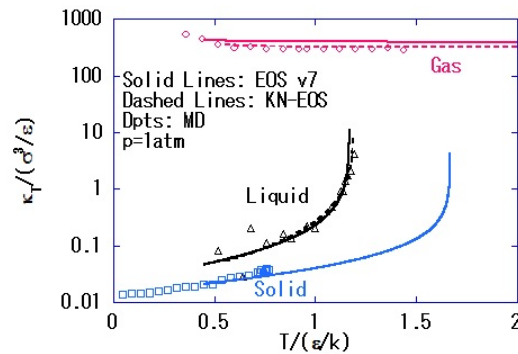


Fig.22 The isothermal compressibility, κ_T , as a function of temperature at $p = 1$ atm. Comparison of EOS v7 results are compared with previous simulation results [11] and the present MD simulations for the solid phase at $p = 1.2$ atm.

Figure 23 shows the heat capacity under constant pressure (C_p) at $p = 1$ atm. The heat capacities in the gas and solid phases are in reasonable agreement with the results obtained by MD simulations at $p = 1.2$ atm. For C_p in the liquid phase, the calculated EOS v7 values are lower than those obtained by the MD simulation and the KN-EOS [11].

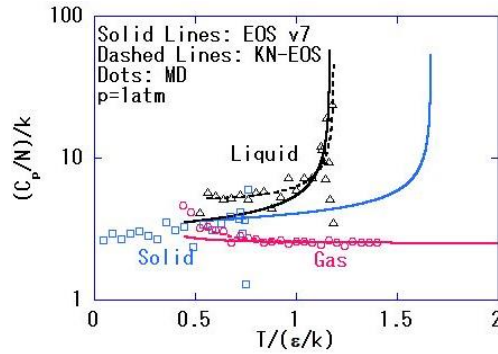


Fig.23 Heat capacity at constant pressure per molecule, C_p/N , as a function of temperature at $p = 1$ atm. EOS v7 results are compared with previous simulation results [11] and the present MD simulations at $p = 1.2$ atm.

6. THERMODYNAMIC CONSISTENCIES

Thermodynamic consistencies were examined using the following thermodynamic equation [1]:

$$(C_p - C_v) \frac{1}{N} = \frac{\alpha^2 TV}{\kappa_T N} \quad (31)$$

The LHS and RHS of Eq. (31) are shown in Fig. 24 for the three phases at $p = 1$ atm. No specific thermodynamic inconsistencies were identified.

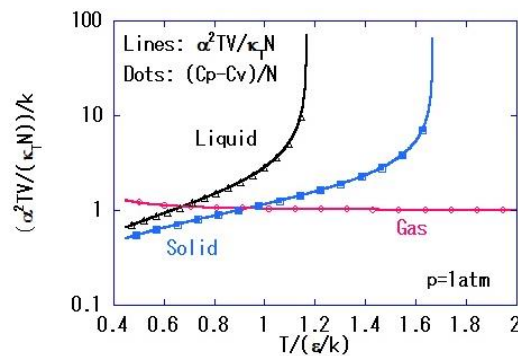


Fig.24 Thermodynamic consistency test (see Eq. (31)).

7. NUMERICAL CALCULATIONS

Several worksheets were prepared to perform the numerical calculations, as shown in Table 4. To obtain plots (such as that shown in Fig. 6), thermodynamic quantities were calculated as functions of $v = V/N$ and T using worksheet functions [23]. The equation $p(v, T_0) = p_0$ was solved with respect to the volume (v) for a given temperature (T_0) and pressure (p_0) using Goal Seek in Microsoft Excel in the second worksheet. These worksheets are available upon request to the author (YK) and are also provided as attached files [24].

Table 4. Worksheets employed for phase transition calculations.

File name	Purpose	Example of figures
EOSv7_T=1.00.xlsx	G/N vs. p plot	Figs. 6–14
EOSv7_p=p0.xlsm	solve $p(V, T_0) = p_0$	Figs. 15–24

8. CONCLUSIONS

The phase transitions among the three phases of the Lennard–Jones system may be calculated with moderate accuracy using our EOS v7 for a perfect solid and liquid, as represented by Eqs. (12) – (17). The EOS for a perfect solid and liquid have a simple analytic form based on the harmonic oscillator approximation. We expect that this set of EOS may be employed for teaching thermodynamics in physical chemistry courses.

ACKNOWLEDGMENT

The authors would like to thank the Research Center for Computing and Multimedia Studies of Hosei University for the use of computer resources.

REFERENCES

- [1] P. W. Atkins, *Physical Chemistry*, Oxford Univ. Press, Oxford (1998).
- [2] Y. Kataoka and Y. Yamada, *J. Comput. Chem. Jpn.*, **10**, 98 (2011).
- [3] Y. Kataoka and Y. Yamada, *J. Comput. Chem. Jpn.*, **11**, 81 (2012).
- [4] Y. Kataoka and Y. Yamada, *J. Comput. Chem. Jpn.*, **11**, 165 (2012).
- [5] Y. Kataoka and Y. Yamada, *J. Comput. Chem. Jpn.*, **11**, 174 (2012).
- [6] Y. Kataoka and Y. Yamada, *J. Comput. Chem. Jpn.*, **12**, 101 (2013).
- [7] Y. Kataoka and Y. Yamada, *J. Comput. Chem. Jpn.*, **12**, 181 (2013).
- [8] Y. Kataoka and Y. Yamada, “Thermodynamics and molecular dynamic simulations of three-phase equilibrium in argon (v6)” submitted to Bulletin of Research Center for Computing and Multimedia Studies, Hosei University.
- [9] M. P. Allen and D. J. Tildesley, *Computer Simulation of Liquids*, Clarendon Press, Oxford (1992).
- [10] J. K. Johnson, J. A. Zollweg and K. E. Gubbins, *Mol. Phys.*, **78**, 591 (1993).
- [11] J. Kolafa and I. Nezbeda, *Fluid Phase Equilib.*, **100**, 1 (1994).
- [12] M. A. van der Hoef, *J. Chem. Phys.*, **113**, 8142 (2000).
- [13] M. A. van der Hoef, *J. Chem. Phys.*, **117**, 5092 (2002).
- [14] J. -P. Hansen and L. Verlet, *Phys. Rev.*, **184**, 151-161 (1969).
- [15] D. A. Kofke, *J. Chem. Phys.*, **98**, 4149-4162 (1993).
- [16] R. Agrawal and D. A. Kofke, *Mol. Phys.*, **85**, 43-59 (1995).
- [17] H. Okumura and F. Yonezawa, *J. Chem. Phys.*, **113**, 9162 (2000).
- [18] H. Okumura and F. Yonezawa, *J. Phys. Soc. Jpn.*, **70**, 1990 (2001).
- [19] M. A. Barroso and A. L. Ferreira, *J. Chem. Phys.*, **116**, 7145 (2002).
- [20] A. Ahmed and R. J. Sadus, *J. Chem. Phys.*, **131**, 174504 (2009).
- [21] F. Cuadros, I. Cachadiña, W. Ahamuda, *Molec. Engineering*, **6**, 319 (1996).
- [22] J. S. Rowlinson and F.L. Swinton, *Liquids and Liquid Mixtures*, Butterworth, London, (1982).
- [23] EOSv7_T=1.00.xlsx
- [24] EOSv7_p=p0.xlsm